Russ. J. Numer. Anal. Math. Modelling, Vol. 26, No. 2, pp. 161–178 (2011)
DOI 10.1515/ RJNAMM.2011.009

Numerical simulation of the North Atlantic – Arctic Ocean – Bering Sea circulation in the 20th century

S. N. MOSHONKIN*, G. V. ALEKSEEV†, A. V. BAGNO*, A. V. GUSEV*, N. A. DIANSKY*, and V. B. ZALESNY*

Abstract — A model of the joint circulation of the North Atlantic, the Arctic Ocean, and the Bering Sea is presented with the resolution of 0.25° in latitude and longitude. The numerical technique of solving this problem and the organization of numerical experiments are described. Numerical calculations have been performed using this model for the period of 1958–2006. The results are compared with observation data and with the results of simulation by other models. Model estimates of the evolution of the Atlantic water incoming into the Arctic basin through the Fram Strait and the Barents Sea are presented. A positive trend of Atlantic water incoming into the Arctic basin through the Fram Strait is revealed. The evolution of the fresh water layer thickness in the Beaufort Gyre is considered. Three periods of increased thickness correlated with increased anticyclonic vorticity are pointed out: 1960s, 1980s, and the period from 1999 until now. The evolution of the anticyclonic vorticity is ahead of the changes in the fresh water layer thickness by 1.75 years. Long-term positive trends of fresh water layer thickness and the anticyclonic field vorticity in the Beaufort Gyre have been observed from the middle of 1970s. This period is characterized by a negative model trend of the ice area in the Arctic, which corresponds to observation data.

An important issue in the simulation of the global ocean circulation is the reproduction and analysis of its structure and variability in the Northern Hemisphere. The joint circulation and interaction of water of the three oceans: Atlantic, Arctic, and Pacific is significant from the viewpoint of the Earth climate variability.

The inflow of Atlantic water into the Arctic Ocean (AO) is part of the global oceanic conveyor linking the oceans by heat, salt, and fresh water transport. Atlantic water arrives from the North Atlantic (NA), spreads in the area of the Norwegian, Greenland, and Barents Seas and penetrates into the Arctic basin, where it occupies the intermediate layer. Atlantic water is an important source of heat and salt in the Arctic basin. The presence of Atlantic water stimulates mixing, including deep convection and formation of new water mass. One of the criteria for models of ocean circulation and sea ice evolution in the Arctic Ocean is the reproduction of the Atlantic water spread and its inter-annual and decennial variability [19].

Another criterion is the ability to reproduce the characteristics of the upper layer,

*Institute of Numerical Mathematics, Russian Academy of Sciences, Moscow 119333, Russia

†Arctic and Antarctic Research Institute, St. Peterburg 199397, Russia

The work was supported by the Russian Foundation for Basic Research (projects 09–05–00266-a, 09–05–00232, 09–05–13545-off, and 09–05–01231-a) and by the Ministry of Science and Education of Russian Federation (GK 14.740.11.0358, 14.740.11.0408, 16.740.11.0359).

in particular, the change of the fresh water concentration in AO [2]. The content of fresh water in AO changes in the course of years and depends on water exchange between the oceans, on the water inflow due to the river runoff, on precipitation, and on ice formation and breakup; this content is distributed over the water area quite nonuniformly [17]. Such circulation phenomenon as the Beaufort Gyre (BG) plays a significant role in the fresh water dynamics in AO and accumulates a considerable mass of such water.

A number of models of ocean circulation and sea ice evolution have been developed. These models differ in their physical parameterizations, the use of different vertical coordinates, numerical techniques, etc. Calculations performed with these models show noticeable distinctions in the reproduction of the ocean and ice circulation structure. The cause of those distinctions and the way of removing them were not clear, which initiated a special project for comparison of the models of the AO (AOMIP). The ultimate goal of this project is to clarify the ability of models to reproduce seasonal, inter-annual, and decennial changes in the fields of the AO and to understand the dependence of a model solution on the variation of boundary conditions.

Below we describe the mathematical model developed at the Institute of Numerical Mathematics (INM) of the RAS for the reproduction of the joint thermohaline circulation of the NA and AO water. The numerical solution technique and also the statement and results of the numerical experiment are described. The aim of this work is to represent the penetration of NA water into AO, the propagation of fresh water over the area of the AO, and the change of fresh water content in the BG using this model. The results of calculations are compared with observation data and simulation results obtained from other models.

1. Mathematical model of the circulation of the North Atlantic–Arctic Ocean – Barents Sea in the σ-system of coordinates

Let us write the equations of the large-scale ocean circulation in the σ-system of coordinates with the normalized depth $\sigma = (z-\zeta)/(H-\zeta)$. We have [1, 23]:

$$Z_\sigma \frac{du}{dt} - Z_\sigma (l+\xi)\, v = -\frac{Z_\sigma}{\rho_0 r_x}\left[\frac{\partial}{\partial x}\left(p - \frac{g}{2}\rho Z\right) + \frac{g}{2}\left(\rho\frac{\partial Z}{\partial x} - Z\frac{\partial \rho}{\partial x}\right)\right] + D_u u$$

$$Z_\sigma \frac{dv}{dt} + Z_\sigma (l+\xi)\, u = -\frac{Z_\sigma}{\rho_0 r_y}\left[\frac{\partial}{\partial y}\left(p - \frac{g}{2}\rho Z\right) + \frac{g}{2}\left(\rho\frac{\partial Z}{\partial y} - Z\frac{\partial \rho}{\partial y}\right)\right] + D_v v$$

$$\frac{\partial}{\partial \sigma}\left(p - \frac{g}{2}\rho Z\right) = \frac{g}{2}\left(\rho\frac{\partial Z}{\partial \sigma} - Z\frac{\partial \rho}{\partial \sigma}\right)$$

$$-\frac{\partial \zeta}{\partial t} + \frac{1}{r_x r_y}\left[\frac{\partial}{\partial x}(Z_\sigma r_y u) + \frac{\partial}{\partial y}(Z_\sigma r_x v)\right] + \frac{\partial \omega}{\partial \sigma} = 0 \qquad (1.1)$$

$$\frac{\partial Z_\sigma T}{\partial t}+\frac{1}{r_y r_x}\frac{\partial}{\partial x}\left(Z_\sigma r_y uT\right)+\frac{1}{r_x r_y}\frac{\partial}{\partial y}\left(Z_\sigma r_x vT\right)+\frac{\partial}{\partial \sigma}(\omega T)=D_T T+R_T$$

$$\frac{\partial Z_\sigma S}{\partial t}+\frac{1}{r_y r_x}\frac{\partial}{\partial x}\left(Z_\sigma r_y uS\right)+\frac{1}{r_x r_y}\frac{\partial}{\partial y}\left(Z_\sigma r_x vS\right)+\frac{\partial}{\partial \sigma}(\omega S)=D_S S$$

$$\rho=\tilde{\rho}\left(T+\bar{T},S+\bar{S},p\right)-\tilde{\rho}\left(\bar{T},\bar{S},\rho_0 gZ\right)$$

$$Z=(H-\zeta)\,\sigma+\zeta.$$

Here (x,y) is a bipolar orthogonal system of coordinates on a sphere with arbitrary positions of the polar points, Z is the ordinary vertical coordinate, u,v,w are the components of the velocity vector, p is the pressure, ρ is the density deviation from the given distribution along the vertical direction, $\tilde{\rho}\left(T+\bar{T},S+\bar{S},p\right)$ is the given function of the sea water state, T is the deviation of the potential temperature from the given value $\bar{T}$, S is the salinity deviation from the given value $\bar{S}$, ρ_0 is the reference density, $\rho_0\approx 1$, D_u, D_v, D_T, D_S, R_T are the terms describing the turbulent exchange and the penetrating solar radiation, l is the Coriolis parameter, r_x, r_y are the metric coefficients depending on the choice of the coordinate system, g is the acceleration of gravity. In addition,

$$\frac{\mathrm{d}}{\mathrm{d}t}=\frac{\partial}{\partial t}+\frac{u}{r_x}\frac{\partial u}{\partial x}+\frac{v}{r_y}\frac{\partial u}{\partial y}+\frac{\omega}{Z_\sigma}\frac{\partial u}{\partial \sigma},\quad \omega=w-\left(\frac{\partial Z}{\partial t}+\frac{u}{r_x}\frac{\partial Z}{\partial x}+\frac{v}{r_y}\frac{\partial Z}{\partial y}\right) \tag{1.2}$$

$$Z=(H-\zeta)\,\sigma+\zeta,\quad Z_\sigma\equiv\frac{\partial Z}{\partial \sigma}. \tag{1.3}$$

Additional notations and definitions including the forms of the state equation and turbulent exchange operators can be found in [3, 23]. Here are some remarks concerning physical parameterizations and boundary and initial conditions.

We take a bipolar orthogonal system as a new coordinate system instead of the ordinary geographic one. The poles of the new system are positioned beyond the calculation domain on the geographic equator at the points with the coordinates 120°W and 60°E.

The horizontal turbulent momentum exchange is described by diffusion operators of the second and fourth orders for the horizontal velocity components along the surfaces $\sigma=$const. Two methods can be used for the parameterization of the heat and salt turbulent exchange in the model. The first method consists in the application of a second-order operator with mixed derivatives [3, 23]. In this case the exchange is described by a diffusion process along the 'geopotential' surfaces $Z=$const. The second method consists in the application of the diffusion operator along the isopycnic surfaces $\rho=$const.

The vertical momentum, heat, and salt turbulent exchange is described by a second-order operator. The vertical turbulence coefficients are calculated according to the chosen parameterization [15, 16]. The process of deep convection under unstable stratification of the potential density is parameterized by the increase in the vertical exchange coefficients by several orders [3, 23].

If the turbulent exchange (of the momentum, heat, and salt) is described by a second-order operator, then the boundary conditions for system of equations (1.1) have the following form.

On the free ocean surface $\sigma = 0$ we have

$$\frac{\partial u}{\partial \sigma} = -Q_u^0, \quad \frac{\partial v}{\partial \sigma} = -Q_v^0, \quad \omega = 0, \quad p = p_{\text{atm}} \tag{1.4}$$

$$\frac{\partial T}{\partial \sigma} = -Q_T^0, \quad \frac{\partial S}{\partial \sigma} = -Q_S^0. \tag{1.5}$$

On the bottom $\sigma = 1$ we have

$$\frac{\partial u}{\partial \sigma} = R_u, \quad \frac{\partial v}{\partial \sigma} = R_v, \quad \omega = 0 \tag{1.6}$$

$$\frac{\partial T}{\partial n} = 0, \quad \frac{\partial S}{\partial n} = 0. \tag{1.7}$$

Condition (1.7) describes the absence of heat and salt flow on the bottom. In the σ-system of coordinates it has the form of a skew derivative [23].

The conditions of nonpercolation and the absence of heat and salt flows are posed on the rigid shore boundary. On the liquid boundary, the values of the velocity, temperature, and salinity are given.

The initial conditions for (1.1) are the following:

$$u = u^0, \quad v = v^0, \quad \zeta = \zeta^0, \quad T = T^0, \quad S = S^0. \tag{1.8}$$

2. Numerical method of solving the problem

The numerical solution of problem (1.1)–(1.8) is performed by the method of multicomponent splitting [12, 13, 24]. Let us describe the scheme of splitting with respect to physical processes we use here.

Suppose we have to solve equations (1.1) in the time interval $t_j < t < t_{j+1}$ with the corresponding boundary conditions.

Divide the operator of system (1.1) into two subsystems: the transport–diffusion of substances and the adaptation of the flow and density fields. We have

the subsystem of transport–diffusion

$$Z_\sigma \frac{\mathrm{d}u}{\mathrm{d}t} = D_u u$$

$$Z_\sigma \frac{\mathrm{d}v}{\mathrm{d}t} = D_v v \tag{2.1}$$

$$\frac{\partial Z_\sigma T}{\partial t} + \frac{1}{r_y r_x}\frac{\partial}{\partial x}(Z_\sigma r_y u T) + \frac{1}{r_x r_y}\frac{\partial}{\partial y}(Z_\sigma r_x v T) + \frac{\partial}{\partial \sigma}(\omega T) = D_T T + R_T$$

$$\frac{\partial Z_\sigma S}{\partial t}+\frac{1}{r_y r_x}\frac{\partial}{\partial x}\left(Z_\sigma r_y u S\right)+\frac{1}{r_x r_y}\frac{\partial}{\partial y}\left(Z_\sigma r_x v S\right)+\frac{\partial}{\partial\sigma}(\omega S)=D_S S$$

and the subsystem of adaptation of the flow and density fields

$$\begin{gathered}
Z_\sigma\frac{\partial u}{\partial t}-Z_\sigma(l+\xi)v=-\frac{Z_\sigma}{\rho_0 r_x}\left[\frac{\partial}{\partial x}\left(p-\frac{g}{2}\rho Z\right)+\frac{g}{2}\left(\rho\frac{\partial Z}{\partial x}-Z\frac{\partial\rho}{\partial x}\right)\right]\\
Z_\sigma\frac{\partial v}{\partial t}+Z_\sigma(l+\xi)u=-\frac{Z_\sigma}{\rho_0 r_y}\left[\frac{\partial}{\partial y}\left(p-\frac{g}{2}\rho Z\right)+\frac{g}{2}\left(\rho\frac{\partial Z}{\partial y}-Z\frac{\partial\rho}{\partial y}\right)\right]\\
\frac{\partial}{\partial\sigma}\left(p-\frac{g}{2}\rho Z\right)=\frac{g}{2}\left(\rho\frac{\partial Z}{\partial\sigma}-Z\frac{\partial\rho}{\partial\sigma}\right)\qquad(2.2)\\
-\frac{\partial\zeta}{\partial t}+\frac{1}{r_x r_y}\left[\frac{\partial}{\partial x}\left(Z_\sigma r_y u\right)+\frac{\partial}{\partial y}\left(Z_\sigma r_x v\right)\right]+\frac{\partial\omega}{\partial\sigma}=0\\
\frac{\partial Z_\sigma T}{\partial t}=0,\quad \frac{\partial Z_\sigma S}{\partial t}=0,\quad \rho=\tilde{\rho}\left(T+\bar{T},S+\bar{S},p\right)-\tilde{\rho}\left(\bar{T},\bar{S},\rho_0 g Z\right).
\end{gathered}$$

Solution of the transport–diffusion subsystem. In order to solve the momentum transport–diffusion equations (the first two equations in (2.1)) we once again apply the method of splitting. We perform splitting with respect to separate spatial coordinates. We linearize the transfer operator and represent it in a symmetric form [23]. The system of split equations in particular coordinates has the following form:

$$\begin{gathered}
\frac{\partial Z_\sigma\varphi}{\partial t}+\frac{1}{2r_y r_x}\left[\frac{\partial}{\partial x}\left(Z_\sigma u^j r_y\varphi\right)+Z_\sigma u^j r_y\frac{\partial\varphi}{\partial x}\right]-D_{x,x}\varphi=0\\
\frac{\partial Z_\sigma\varphi}{\partial t}+\frac{1}{2r_y r_x}\left[\frac{\partial}{\partial y}\left(Z_\sigma v^j r_x\varphi\right)+Z_\sigma v^j r_x\frac{\partial\varphi}{\partial y}\right]-D_{y,y}\varphi=0\qquad(2.3)\\
\frac{\partial Z_\sigma\varphi}{\partial t}+\frac{1}{2}\left[\frac{\partial}{\partial\sigma}\left(\omega^j\varphi\right)+\omega^j\frac{\partial\varphi}{\partial\sigma}\right]=D_{\sigma,\sigma}\varphi
\end{gathered}$$

where φ is either u or v. Equations (2.3) with the corresponding boundary conditions are approximated on a staggered grid proposed by V. I. Lebedev [11]. They are linearized in the time step interval $t_j<t<t_{j+1}$ and are solved by an implicit scheme.

In order to solve the transport–diffusion equations for temperature and salinity (the last two equations in (2.1)), we apply the method of splitting of another type. We linearize the problem in the interval $t_j<t<t_{j+1}$ and represent its operator as a sum of 'n' equal parts. For the sake of brevity, assume $R_T=0$. We have

$$\frac{\partial Z_\sigma\varphi}{\partial t}+\frac{1}{n}\underbrace{\left[\left(C_\varphi-D_\varphi\right)+\cdots+\left(C_\varphi-D_\varphi\right)\right]}_{n}\varphi=0\qquad(2.4)$$

$$C_\varphi \varphi = \frac{1}{r_x r_y}\frac{\partial}{\partial x}\left(Z_\sigma r_y u^j \varphi\right) + \frac{1}{r_x r_y}\frac{\partial}{\partial y}\left(Z_\sigma r_x v^j \varphi\right) + \frac{\partial}{\partial \sigma}\left(\omega^j \varphi\right)$$

where φ is either T or S.

Equations (2.4) are approximated in spatial coordinates on a staggered grid of V. I. Lebedev [11] and are solved by an implicit scheme. The splitting scheme of equations (2.4) is reduced to the solution of the following chain of identical equations in the interval $t_j < t < t_{j+1}$:

$$\frac{\partial Z_\sigma \varphi}{\partial t_1} + \left(C_\varphi - D_\varphi\right)\varphi = 0, \quad \cdots \quad , \quad \frac{\partial Z_\sigma \varphi}{\partial t_1} + \left(C_\varphi - D_\varphi\right)\varphi = 0 \tag{2.5}$$

$$t_1 = \frac{t}{n}.$$

It can be seen that each equation of (2.5) is solved in an n-time reduced time interval. This technique allows us to improve the stability of calculations.

Solution of the subsystem of adaptation of the flow and density fields. We linearize equations of adaptation of the flow and density fields (2.2) in the interval $t_j < t < t_{j+1}$. We get a problem for determination of the velocity vector and the sea level from the known density field. It is solved in the following way [24]. The field of the horizontal flows is represented there as the mean over the vertical direction and the deviation from the mean:

$$u = \bar{u} + u', \quad v = \bar{v} + v', \quad \bar{a} = \int_0^1 a \mathrm{d}\sigma. \tag{2.6}$$

Using this decomposition and taking into account that the vertical velocity ω equals zero on the upper and lower boundaries, system (2.2) can be split into two subsystems. The first subsystem describes the contribution of metric summands

$$\frac{\partial u}{\partial t} - \xi v = 0, \quad \frac{\partial v}{\partial t} + \xi u = 0. \tag{2.7}$$

The second one corresponds to the calculation of the flow field from the known density field

$$\frac{\partial u}{\partial t} - lv = \frac{g}{2r_x}\frac{\partial \zeta}{\partial x} + \frac{g}{2\rho_0 r_x}\left[\left(\rho\frac{\partial Z}{\partial x} - Z\frac{\partial \rho}{\partial x}\right) - \frac{\partial}{\partial x}\int_0^\sigma \left(\rho\frac{\partial Z}{\partial \sigma_1} - Z\frac{\partial \rho}{\partial \sigma_1}\right)\mathrm{d}\sigma_1\right]$$
$$- \frac{1}{\rho_0 r_x}\frac{\partial p_{\mathrm{atm}}}{\partial x}$$

$$\frac{\partial v}{\partial t}+lu=\frac{g}{2r_y}\frac{\partial \zeta}{\partial y}+\frac{g}{2\rho_0 r_y}\left[\left(\rho\frac{\partial Z}{\partial y}-Z\frac{\partial \rho}{\partial y}\right)-\frac{\partial}{\partial y}\int_0^{\sigma}\left(\rho\frac{\partial Z}{\partial \sigma_1}-Z\frac{\partial \rho}{\partial \sigma_1}\right)\mathrm{d}\sigma_1\right]$$

$$-\frac{1}{\rho_0 r_y}\frac{\partial p_{\mathrm{atm}}}{\partial y}-\frac{\partial \zeta}{\partial t}+\frac{1}{r_x r_y}\left[\frac{\partial}{\partial x}(Z_\sigma r_y \bar{u})+\frac{\partial}{\partial y}(Z_\sigma r_x \bar{v})\right]=0 \qquad (2.8)$$

$$\omega=\frac{1}{r_x r_y}\int_{\sigma}^{1}\left\{\frac{\partial}{\partial x}\left[Z_{\sigma_1} r_y (u-\bar{u})\right]+\frac{\partial}{\partial y}\left[Z_{\sigma_1} r_x (v-\bar{v})\right]\right\}\mathrm{d}\sigma_1.$$

The functions sought for here are the components of the velocity vector u, v, ω and the sea level ζ. The sea level $\zeta(x,y,t)$ is a function not dependent on the vertical coordinate σ. This allows us to separate the problem of the calculation of the level and the mean in the vertical direction velocity components as an independent module

$$\frac{\partial \bar{u}}{\partial t}-l\bar{v}=\frac{g}{2r_x}\frac{\partial \zeta}{\partial x}$$

$$\frac{\partial \bar{v}}{\partial t}+l\bar{u}=\frac{g}{2r_y}\frac{\partial \zeta}{\partial y}-\frac{\partial \zeta}{\partial t}+\frac{1}{r_x r_y}\left[\frac{\partial}{\partial x}(Z_\sigma r_y \bar{u})+\frac{\partial}{\partial y}(Z_\sigma r_x \bar{v})\right]=0. \qquad (2.9)$$

Equations (2.9) with the nonpercolation condition on the rigid boundary are approximated on a staggered grid [11]. An implicit scheme is used in the time direction, the corresponding system of algebraic equations is solved by a direct algorithm in terms of (u^h, v^h, ζ^h).

3. Statement of numerical experiment

The calculation domain includes the North Atlantic from 20°S (including the Mediterranean and Baltic Seas), the Arctic Ocean (AO), and the north part of the Pacific Ocean, i.e., the Bering Sea. In the Pacific Ocean the liquid boundary goes over the straits of the Aleutian Islands. The model has the spatial resolution of (1/4)° in the longitude and latitude. This resolution admits the simulation of synoptic ocean dynamics in mid-latitudes [6].

The ocean bottom topography is taken from the ETOPO5 data. The model depth is bounded by the minimal value of 5 m. The vertical direction is divided into 27 σ-levels with a finer resolution in the upper ocean layer. Monthly climatic values of temperature and salinity are posed on the liquid boundaries from the surface to the bottom for each integration step according to the data of [22].

The runoff of the main rivers influencing the salinity distribution is taken into account similar to the precipitation near the river outfalls [7]. In this series of experiments the river runoff into the Arctic Ocean is given by the mean annual climatic value, i.e., by a single value for each river.

The coefficients of large-scale lateral diffusion for temperature and salinity are taken equal to each other (as the functions of the depth and latitude) in the numerical experiments; their maximal value is equal to 2×10^6 cm^2/s and is attained on

the physical equator; these functions smoothly decrease by half with the depth and toward higher latitudes. A fourth-order operator is used as the operator of lateral viscosity.

The vertical viscosity and diffusion coefficients are chosen according to the parameterization of Monin–Obukhov [9]. The convective instability is parameterized by setting the large value of 500 cm^2/s for the vertical coefficients of viscosity and diffusion. The ocean circulation model includes an adapted model of sea ice dynamics and thermodynamics [8].

The main purpose of the numerical experiments was to study the ability of the model to reproduce the structure of mean monthly ocean fields. These are the fields of temperature, salinity, flow velocity, sea level, and some other characteristics. The boundary conditions on the ocean surface were posed as the flows of momentum, heat, and moisture. They were calculated using atmospheric characteristics from the CORE data. The CORE array was especially prepared for experiments with models of ocean and ice evolution within the CLIVAR Programme [10]. The array presents flows of long- and short-wave radiation on the sea level with the discreteness of one day. The air humidity, pressure, and temperature on the sea level are given with the discreteness of six hours. The wind velocity components at the level of 10 meters above the ocean level are also given with the discreteness of six hours. The intensity of atmospheric precipitation is given with the discreteness of one month. The river runoff in the CORE array in given by its mean annual climatic value. The wind friction and the flows of explicit and hidden heat are calculated by bulk-formulas [10]. The calculation of explicit and hidden heat flows uses the model temperature of the ocean surface.

In the equations for heat and salt, the total flows of heat and moisture are used as the boundary condition on the surface. The moisture budget consists of precipitation minus evaporation. The heat budget is the sum of the radiation budget plus the flows of the explicit and hidden heat. The radiation budget for short-wave radiation takes into account its penetration power.

The following additional relaxation term is introduced in the calculation of fresh water flows:

$$F_r = -\gamma_S (S_0 - S_1)/S_1 \tag{3.1}$$

where $\gamma_S = 2.0 \times 10^{-3}$ cm/s; S_1 is the salinity on the first model horizon, S_0 is the given salinity [22].

The experiments with the boundary conditions described above were performed in two stages. At the first stage, the climatic three-dimensional winter fields of the ocean temperature and salinity and the state of rest were given as the initial conditions [22]. Then we performed the calculation with the step of one hour for 20 annual cycles with the boundary conditions calculated from the CORE data for 1958. As the result, a state close to equilibrium was formed for all model characteristics representing the seasonal course of 1958.

At the second stage, we performed calculations for the period from 1959 to 2006. The fields corresponding to the final calculation step of December 31, 1958 were taken as the initial conditions. The atmosphere forcing was given according

to the CORE data for the period from 1959 to 2006. The time step at the first and second stages was equal to one hour.

4. Comparison of results of numerical experiments with observation data and calculations by other models

Figure 1 shows the circulation field of the Greenland, Norwegian, and Barents Seas reproduced in the numerical experiment. Figure 2 demonstrates the circulation field in the Arctic Ocean. The model circulation of the upper layer of the Arctic basin has such well-known elements as the Transpolar Drift and the anticyclonic Beaufort Gyre (Fig. 2).

We compared flow fields obtained from our model with circulation fields reproduced in the model with a higher resolution $1/12^\circ \times 1/12^\circ \times 45$ [14]. A high degree of similarity was observed. There is a correspondence in the structure of the West Spitsbergen Current and its recirculation in the region of the Fram Strait; of the East

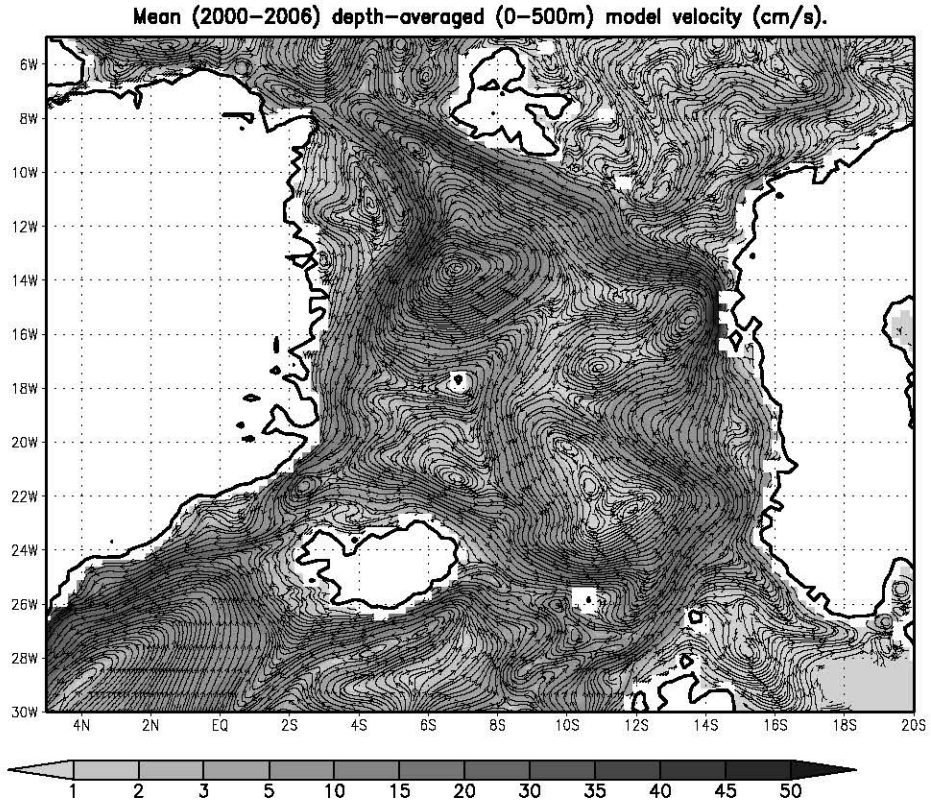

Figure 1. Current field streamlines averaged for the layer of 0 – 500 m in period of 2000 – 2006 in the Greenland, Norwegian, and Barents Seas. The coordinates are model. The absolute value of the velocity is shown by the intensity of the background.

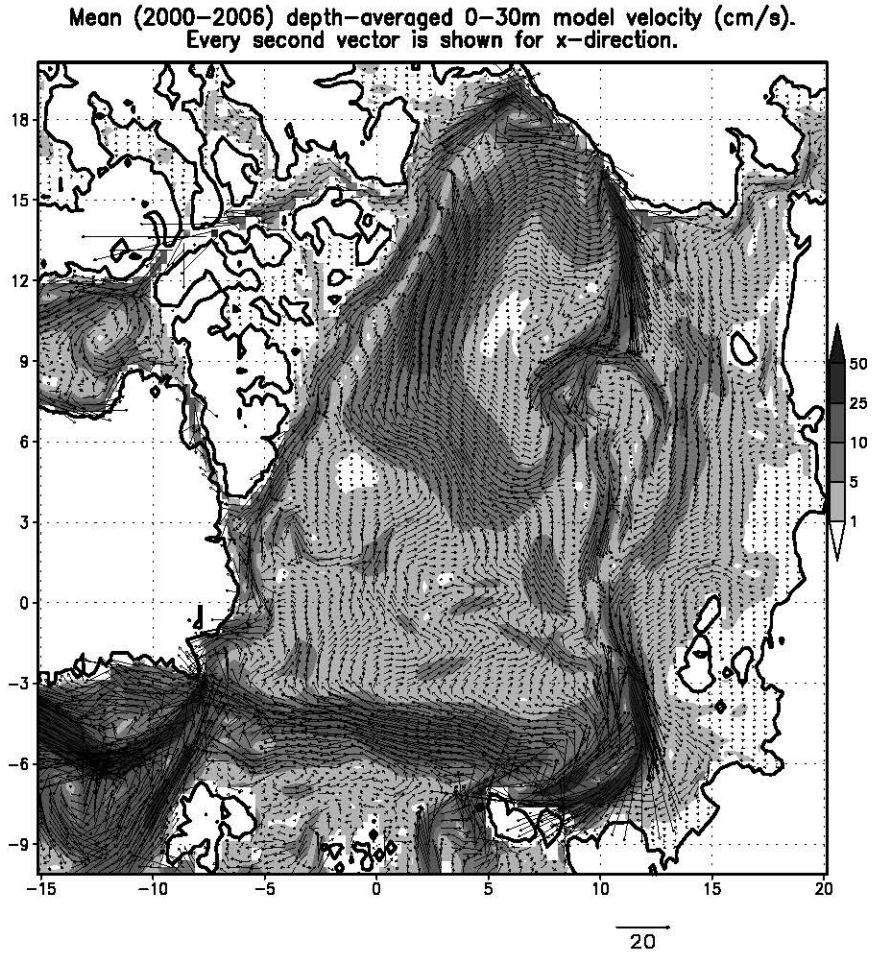

Figure 2. Current field in the Arctic basin (vectors, averaging in the layer of 0 – 30 m for the period of 2000 – 2006). The coordinates are model. The absolute value of the velocity is shown by the intensity of the background.

Greenland and Nordkap Currents; intensive water outflow from the Barents Sea into the Arctic basin in the region of the St. Anna Trough. A good agreement is observed in the reproduction of quasistationary large-scale eddies.

Figure 3 shows the transport of Atlantic water between the Spitsbergen and the Norway (Barents Sea Opening) and through the Fram Strait. The transport of Atlantic water is characterized by a seasonal process with its maximal values in winter and spring months (in Fig. 3 the seasonal process is removed). The inter-annual variability is very high. The long-period quasidecade variability is also visible.

We do not reveal significant long-term trends in the water transport from the Norwegian Sea into the Barents Sea. The mean Atlantic water transport amount at the cross-section at 20° E for the period of 1958 – 2006 equals 4.41 Sv (1 Sv =

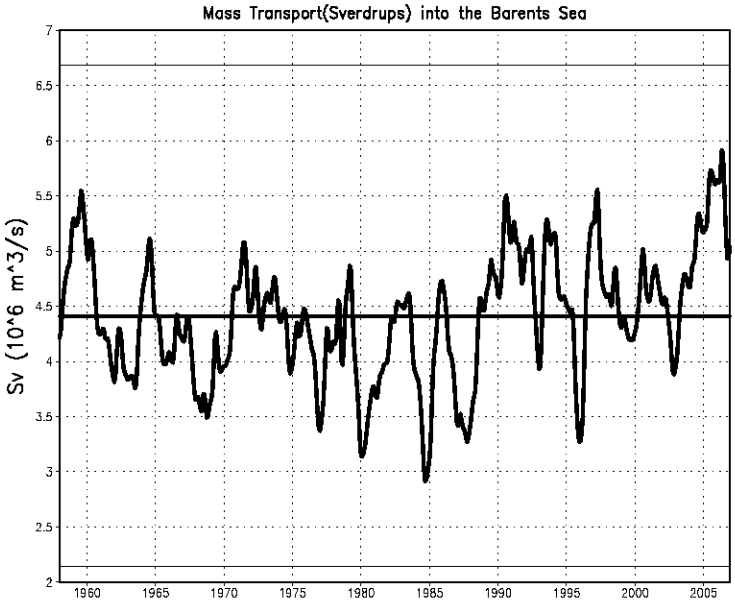

(a)

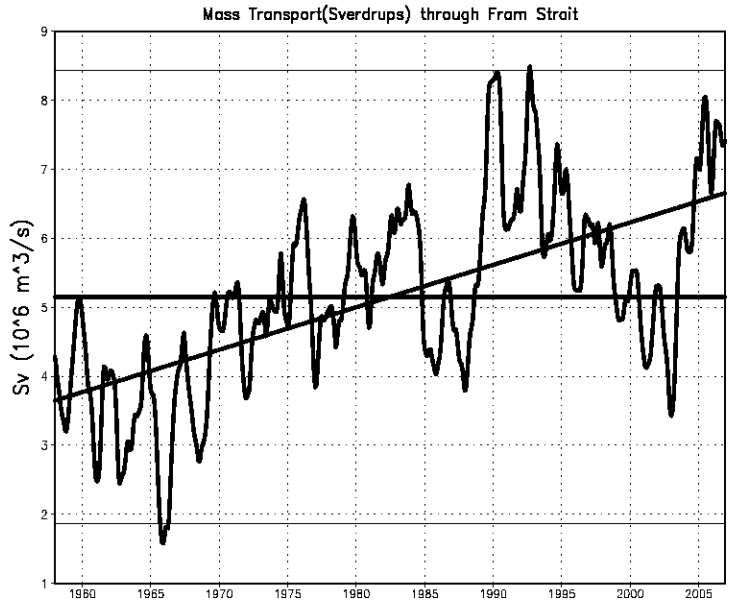

(b)

Figure 3. Evolution of water transport in Sverdrups (1 Sv = 10^6 m^3/s): (a) from the Norwegian Sea into the Barents Sea; (b) from the Greenland Sea to the Arctic basin through the Fram Strait. The annual process is filtered. Horizontal lines indicate the mean and the mean plus/minus MSD for the period of I.1958–XII.2006. Fragment (b) shows the transport velocity growth trend in time.

10^6 m^3/s) (Fig. 3a). This value is close to the estimate presented in [14]. The mean square deviation of the water transport is equal to 2.27 Sv.

There exist representative observation data for the flow velocity, temperature, and salinity in the Fram Strait for the period from September 1997 until August 1999 [5]. The comparison of the calculation results with these data shows their qualitative and quantitative coincidence. Thus, similar to the data, the barotropic component dominates in the West Spitsbergen Current, but in the East Greenland Current the baroclinic and barotropic components have comparable magnitudes. The mean biannual velocity of the West Spitsbergen Current is close to the observation data. In particular, the velocity on the Spitsbergen continental slope in the layer of 1000–2000 m reaches 8 – 10 cm/s both in the model and in the observation data. In the core of the East Greenland Current positioned in the layer of 300 m from the surface, the velocities are equal to 7 cm/s according to the observation data and to 11 cm/s according to the model. The time trends of water transport directed northward and southward appear to be cophasal in the model and in the observation. The main difference of the calculation results from the observation data is registered near the Greenland continental slope. In this region, the model demonstrates a core of the near-bottom current from the AO in the layer of 1 – 2 km with the maximum velocity of 10 – 11 cm/s. According to the observation data, the velocity here monotonically decreases with the depth and is about 3 – 4 cm/s [5].

A detailed review of the field and model estimates of water transport from the Greenland Sea into AO through the Fram Strait region was given in [14]. These estimates vary within the range of 3 – 8 Sv. It was emphasized that the recirculation of the West Spitsbergen Current in the Fram Strait complicates the determination of the Atlantic water transport into AO. In order to obtain a model estimate of water transport just into the Arctic basin, we choose a cross-section near the Spitsbergen, two degrees to the north from the Fram Strait. A convergence of the currents going after the recirculation into the Arctic basin is seen here.

Figure 3b shows the time variability of water transport from the Greenland Sea into AO in the region of the Fram Strait after recirculation. Note the big magnitudes of the Atlantic water transport in 1990s and in the period of 2004 – 2006. The mean transport in the period of 1958 – 2006 is 5.16 Sv and the mean square deviation is 3.29 Sv. The well expressed positive trend equal to 0.061 Sv/year (Fig. 3a) is the peculiarity representing the evolution of the Atlantic water transport into AO during the last half a century. In average, the transport of Atlantic water into AO by the north branch of the West Spitsbergen Current has increased from 1960s to 2000s by nearly 3 Sv.

5. Evolution of fresh water and vorticity in the Beaufort Gyre

As was said above, one of principal problems of the AO dynamics is the process of accumulation of fresh water in the Beaufort Gyre (BG). The content of fresh water in the upper ocean layer from the surface to the isohaline level $S = 34.8\,^0/_{00}$

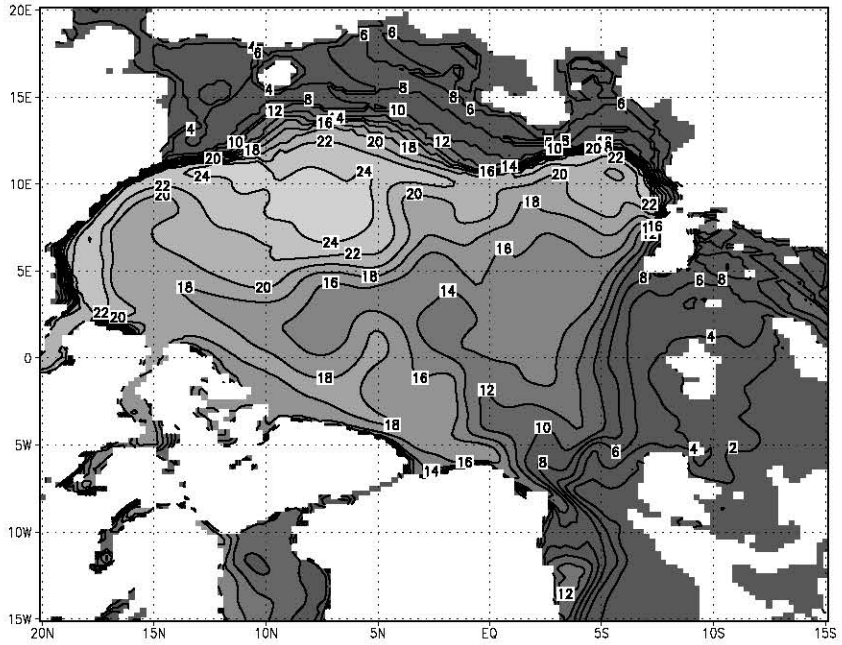

Figure 4. Distribution of the fresh water layer thickness in meters (with respect to 34.8 per mille) in the Arctic basin according to the results of model experiments (mean for years 2000 – 2006).

is calculated in the following way:

$$P_W = \int_0^h \frac{34.8 - S}{34.8} \mathrm{d}z \tag{5.1}$$

where h is the depth (in m) of the isohaline $34.8\,{}^0/_{00}$, S is the salinity in ${}^0/_{00}$.

Figure 4 presents the map of the fresh water layer thickness according to the model for the period of 2000s. The corresponding map obtained by generalization of observation data was presented in [2]. A nearly monotone increase of the fresh water layer thickness from 2 m in the Barents and Kara Seas to 25 m and more in BG is observed both in the observation data and in the model. The main difference is the fact that the model essentially overestimates the fresh water thickness in the Laptev Sea (18 – 20 m in the model and 6 – 8 m according to the data of [2]). However, as a whole, we can point out that the model satisfactory reproduces the spatial structure of the fresh water content in AO and BG.

Consider the long-term joint evolution of fresh water and the vorticity of currents in the central region of the BG. Unfortunately, it is impossible to do that with observation data. Therefore, we consider the results of processing of the numerical experiments.

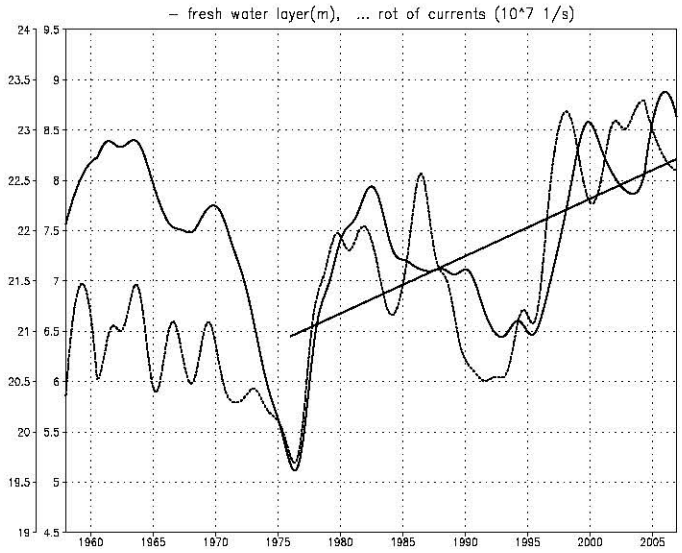

Figure 5. Evolution of the fresh water layer thickness for the period of 1958 – 2006 (from the surface to the depth of isohaline $34.80^0/_{00}$; solid line, left axis, meters) and anticyclonic vorticity of the velocity on the horizon of 10 m (dotted line, right axis, $10^{-7}s^{-1}$). The characteristics are averaged over the central part of the Beaufort Gyre. Time scales exceeding five years are emphasized by filtration in realizations. The positive trend (6 cm/year) of the fresh water layer thickness is shown for the period of 1976 – 2006.

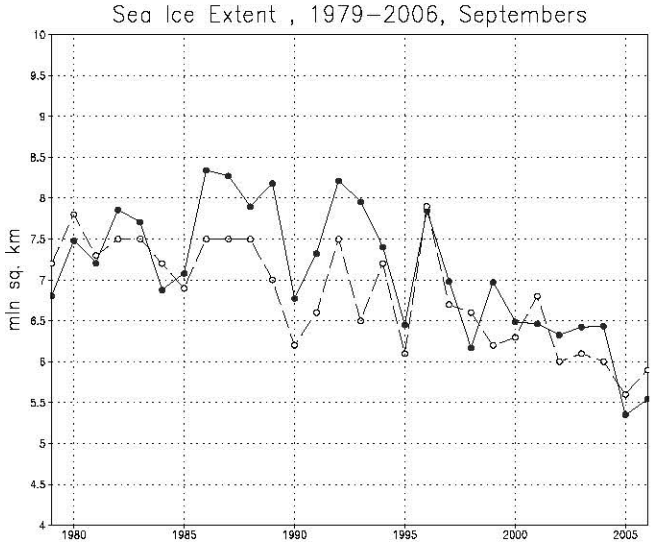

Figure 6. Evolution of the total sea ice extent (millions of square km) in September according to observation data [21] (dashed line) and the model (solid line). Monthly data.

According to one of hypotheses, the main cause of the fresh water accumulation in BG is the Ekman wind pumping under the anticyclonic atmospheric forcing [20]. Here we consider the complete current field including the barotropic and baroclinic wind components. Take a subdomain Ω in the central part of the Beaufort Gyre ($10^\circ \times 10^\circ$ in the model coordinates, see Figs. 2 and 4). Calculate the mean with respect to Ω characteristics of the fresh water content:

$$\overline{P_W} = \frac{1}{\Omega} \int_{\Omega} P_W \mathrm{d}\Omega \tag{5.2}$$

and the mean anticyclonic vorticity of the current field

$$\overline{\omega_z} = \frac{1}{\Omega} \int_{\Omega} \omega_z \mathrm{d}\Omega, \quad \omega_z = \frac{\partial v}{\partial x} - \frac{\partial u}{\partial y} \tag{5.3}$$

where (u, v) is the velocity vector on the horizon of 10 m.

Figure 5 shows the time variability of the fresh water thickness and the mean anticyclonic vorticity in the central part of BG. The correlation of these two parameters is clearly seen. The function of correlation between the anticyclonic vorticity of flows and the thickness of the fresh water layer in BG shows that the maximal and reliable correlation (0.68) is attained when the anticyclonic vorticity outruns the fresh water content by a year and nine months (1.75 year). Thus, the model reproduces the positive feedback of the circulation and the fresh water budget in BG at least during the last fifty years. The intensification of anticyclonic circulation in BG, including the thermohaline and wind components, leads to the accumulation of fresh water with the indicated time lag.

The time variability of the Atlantic water transport into AO, the thickness of the fresh water layer, and the vorticity of the currents of BG demonstrate the presence of a quasidecade variability of these characteristics. The results of numerical experiments show the presence of three periods of increase in the fresh water layer thickness and the anticyclonic flow vorticity in BG. These are 1960s, 1980s, and the period from 1999 until now (Fig. 5). Note that the thickness of the fresh water layer had been growing in BG in the period from 1970s to 2000s according to the model results (Fig. 5), this was also pointed out in the observation data [2].

A hypothesis was proposed in [4, 18] that the quasidecade changes are self-oscillations in the ocean–atmosphere system leading to a change of modes in the dominant anticyclonic and cyclonic atmospheric circulation in the Arctic. The change of modes is regulated by the evolution of the gradients of dynamic altitudes and temperatures between the Arctic basin and the Greenland/Norwegian Seas. In particular, the process is marked by the growth or decrease of the Atlantic water inflow into AO [4]. Therefore, in order to estimate the mean statistical time scale of the quasidecade model variability, we calculate the function of the mutual correlation between the Atlantic water inflow through the Fram Strait and the mean vorticity of currents in the upper layer of BG.

Ordering the events according to the principle of advancing in time, we get the following picture. The inflow of Atlantic water outruns the evolution of the vorticity of currents in the BG by 5.58 years (the maximal reliable correlation is 0.71). Taking the scale of 9 months (the advance of the North Atlantic oscillation over the Atlantic water transport) and of 1.75 years (the advance of the anticyclonic vorticity of flows in BG over the fresh water content in BG), we can speak about the time scale of 8 years. The total time scale of such cycle is estimated as 16 years. This estimate is close to the estimates of the corresponding time scales presented in [4]. Thus, according to the results of numerical experiments, the dynamic accumulation of water in BG proceeded for 8 years in average during the last half a century. In the reverse phase, there was a decrease in the anticyclonic vorticity of flows in BG and the outflow of fresh water first from BG and then from AO. This process ought to be accompanied by the formation of salinity anomalies in the sub-Arctic circulation in the North Atlantic.

Above we have given the characteristics of the positive trend of the Atlantic water inflow into AO (Fig. 3b). Similar and reliable trends are revealed for other characteristics. Thus, according to the results of numerical experiments, positive trends both of the fresh water thickness layer (Fig. 5) and of the anticyclonic vorticity of flows in BG have been observed from the middle of 1970s until now. Starting with the second half of 1970s and until now, a steady negative trend of the sea ice extent in the Arctic and sub-Arctic has been marked according to the data of satellite observations [21]. Figure 6 demonstrates the ability of the model to reproduce the total sea ice extent in September. This trend is practically the same in the model and in the observation data. Note here that the sea ice extent has decreased in the whole Arctic by 26.6 % and by 63 % for the Siberian seas in the total period of satellite observations [2]. Thus, the model satisfactory represents the complex of interrelated events in the time scales of several decades.

Conclusion

Using the numerical model of the INM RAS, we have performed the calculations of the joint circulation of the Arctic Ocean, North Atlantic, and Bering Sea for the period from January 1958 to December 2006. A comparison with observation data was performed demonstrating a satisfactory quality of the model reproduction of the flows in the Fram Strait, the distribution of the fresh water thickness in 2000s in the Arctic basin, the time variability of the fresh water thickness in the Beaufort Gyre, and the contemporary evolution of the ice extent.

An analysis of the Atlantic water inflow into the Arctic Ocean was given. It was pointed that the positive trend of 0.061 Sv/year is the characteristic of the long-term evolution of Atlantic water inflow into the Arctic Ocean (during the last half century through the Fram Strait). The model estimations of the amounts of the Atlantic water inflow into the Barents Sea and Arctic basin through the Fram Strait are 4.41 ± 2.27 and 5.16 ± 3.29, respectively.

The model reproduces the positive feedback of the ocean circulation and the fresh water content in the BG. The intensification of anticyclonic circulation in BG

leads to the accumulation of fresh water there with the mean statistical time lag of 1.75 years. Three periods of higher values of the fresh water layer thickness and the anticyclonic current vorticity in the Beaufort Gyre are pointed out. These are the periods of 1960s, 1980s, and from 1999 until now. The mean statistical time scale of the growth and decrease cycles of these interrelated processes is estimated as 16 years, which is close to the existing estimates.

According to the results of numerical experiments, positive trends of the fresh water layer thickness and of the anticyclonic vorticity of currents in the Beaufort Gyre have been observed since mid-1970s until now. Starting from the second half of 1970s and until now, a steady negative trend of the sea ice extent in the Arctic has been observed according to the observation data and to the model.

References

1. V. I. Agoshkov, V. M. Ipatova, V. B. Zalesny, E. I. Parmuzin, and V. P. Shutyaev, Variational observation data assimilation problems for models of general ocean circulation and methods of their solution. *Izv. Akad. Nauk, Fiz. Atmos. Okeana* (2010) **46**, No. 6, 734–770 (in Russian).
2. G. V. Alekseev, A. V. Pnyushkov, N. E. Ivanov, I. M. Ashik, and V. T. Sokolov, Complex estimation of climatic changes in the Marine Arctic with the use of IPY 2007–2008 data. *Problemy Arktiki i Antratktiki* (2009) **81**, No. 1, 7–14 (in Russian).
3. N. A. Diansky, A. V. Bagno, and V. B. Zalesny, Global ocean circulation sigma-model and its sensitivity to the variation of wind friction stress. *Izv. Akad. Nauk, Fiz. Atmos. Okeana* (2002) **38**, No. 4, 537–556 (in Russian).
4. D. S. Dukhovskoy, M. A. Johnson, and A. Proshutinsky, Arctic decadal variability: An auto-oscillatory system of heat and fresh water exchange. *Geophys. Res. Lett.* (2004) **31**, L03302.
5. E. Fahrbach, J. Meinke, S. Osterhus, G. Rohart, U. Schauer, V. Tverberg, and J. Verduin, Direct measurements of volume transports through Fram Strait. *Polar Res.* (2001) **20**, No. 2, 217–224.
6. U. Garternicht and F. Schott, Heat fluxes of the Indian Ocean from a global eddy-resolving model. *J. Geophys. Res.* (1997) **102**, No. C9, 21147–21159.
7. S. M. Griffies, C. Boning, F. O. Bryan, E. P. Chassignet, R. Gerdes, H. Hasumi, A. Hirst, A.-M. Treguier, and D. Webb, Developments in ocean climate modelling. *Ocean Modelling* (2000) **2**, 123–192.
8. N. G. Yakovlev, Joint model of the general ocean circulation and sea ice evolution in the Arctic Ocean. *Izv. Akad. Nauk, Fiz. Atmos. Okeana* (2003) **39**, No. 3, 394–409.
9. V. P. Kochergin, V. I. Klimok, and V. A. Sukhorukov, Uniform ocean layer within the framework of 'differential' models. *Numer. Meth. Solid Mech.* (1977) **8**, No. 5, 102–114.
10. W. G. Large and S. G. Yager, *Diurnal to Decadal Global Forcing for Ocean and Sea-Ice Models: The Data Sets and Flux Climatologies.* Climate and Global Dynamics Division. National Center for Atmospheric Research. Boulder, Colorado, 2004.
11. V. I. Lebedev, Difference analogues of orthogonal decompositions, fundamental differential operators, and basic initial boundary value problems of mathematical physics. *Zh. Vych. Mat. Mat. Fiz.* (1964) **4**, No. 6, 449–465 (in Russian).
12. G. I. Marchuk, *Methods of Numerical Mathematics*. Springer, New York, 1982.
13. G. I. Marchuk, *Splitting Methods*. Nauka, Moscow, 1988 (in Russian).

14. W. Maslowski, D. Marble, W. Walczowski, U. Schauer, J. L. Clement, and A. J. Semtner, On climatological mass, heat, and salt transports through the Barents Sea and Fram Strait from a pan-Arctic coupled ice-ocean model simulation. *J. Geophys. Res.* (2004) **109**, C03032.

15. A. S. Monin and A. M. Obukhov, Dimensionless characteristics of the turbulence in the near-surface layer of the atmosphere. *Dokl. Akad. Nauk SSSR* (1953) **93**, No. 2, 223–226 (in Russian).

16. R. C. Pacanovsky and G. Philander, Parameterization of vertical mixing in numerical models of the tropical ocean. *J. Phys. Oceanogr.* (1981) **11**, 1442–1451.

17. I. V. Polyakov, V. A. Alexeev, G. I. Belchansky, I. A. Dmitrenko, V. V. Ivanov, S. A. Kirillov, A. A. Korablev, M. Steele, L. A. Timokhov, and I. Y. Yashayaev, Arctic ocean fresh water changes over the past 100 years and their causes. *J. Climate* (2008) **21**, No. 2, 364–384.

18. A. Proshutinsky, R. H. Bourke, and F. A. McLaughlin, The role of the Beaufort Gyre in Arctic climate variability: Seasonal to decadal climate scales. *Geophys. Res. Lett.* (2002) **29(23)**, 2100.

19. A. Proshutinsky, J. Yang, R. Krishfield, R. Gerdes, M. Karcher, F. Kauker, C. Koeberle, S. Hakkinen, W. Hibler, D. Holland, M. Maqueda, G. Holloway, E. Hunke, W. Maslowski, M. Steele, and J. Zhang, Arctic Ocean Study: Synthesis of Model Results and Observations. *EOS, Transactions Amer. Geophys. Union* (2005) **86**, No. 40.

20. A. Proshutinsky, R. Krishfield, M.-L. Timmermans, et al., The Beaufort Gyre Fresh Water Reservoir: state and variability from observations. *J. Geophys. Res.* (2009) **114**, C00A10.

21. *Sea Ice Index. Sea Ice Animation Tool.* National Snow and Ice Data Center. 2009. http://nsidc.org/data/seaice_index/archives/image_select.html

22. M. Steele, R. Morley, and W. Ermold, PHC: A global ocean hydrography with a high–quality Arctic Ocean. *J. Climate* (2001) **14**, No. 9, 2079–2087.

23. V. B. Zalesny and A. V. Gusev, Mathematical model of the World Ocean dynamics with algorithms of variational assimilation of temperature and salinity fields. *Russ. J. Numer. Anal. Math. Modelling* (2009) **24**, No. 2, 171–191.

24. V. B. Zalesny, G. I. Marchuk, V. I. Agoshkov, A. V. Bagno, A. V. Gusev, N. A. Diansky, S. N. Moshonkin, R Tamsalu, and E. M. Volodin, Numerical simulation of large-scale ocean circulation based on the multicomponent splitting method. *Russ. J. Numer. Anal. Math. Modelling* (2010) **25**, No. 6, 581–609.